J. Fluid Mech. (2003), *vol.* 474, *pp.* 355–378.
DOI: 10.1017/S0022112002002793 Printed in the United Kingdom

Statistical structure of high-Reynolds-number turbulence close to the free surface of an open-channel flow

By ISABELLE CALMET[1] AND JACQUES MAGNAUDET[2]

[1]Ecole Centrale de Nantes, UMR 6598, 1 rue de la Noe, 44321 Nantes cedex 3, France

[2]Institut de Mécanique des Fluides de Toulouse, UMR 5502, 2 avenue Camille Soula, 31400 Toulouse, France

(Received 21 September 2001 and in revised form 28 August 2002)

Statistical characteristics of turbulence in the near-surface region of a steady open-channel flow are examined using new data obtained in a high-Reynolds-number large-eddy simulation using a dynamic subgrid-scale model. These data, which correspond to a Reynolds number $Re^* = 1280$ based on the total depth and shear velocity at the bottom wall, are systematically compared with those found in available direct numerical simulations in which Re^* is typically one order of magnitude smaller. Emphasis is put on terms involved in the turbulent kinetic energy budget (dominated by dissipation and turbulent transport), and on the intercomponent transfer process by which energy is exchanged between the normal velocity component and the tangential ones. It is shown that the relative magnitude of the pressure–strain correlations depends directly on the anisotropy of the turbulence near the bottom of the surface-influenced layer, and that this anisotropy is a strongly decreasing function of Re^*. This comparison also reveals the Re^*-scaling laws of some of the statistical moments in the near-surface region, especially those involving vorticity fluctuations. Velocity variances, length scales and one-dimensional spectra are then compared with predictions of the rapid distortion theory elaborated by Hunt & Graham (1978) to predict the effect of the sudden insertion of a flat surface on a shearless turbulence. A very good agreement is found, both qualitatively and quantitatively, outside the thin viscous sublayer attached to the surface. As the present high-Reynolds-number statistics have been obtained after a significant number of turnover periods, this agreement strongly suggests that the validity of the Hunt & Graham theory is not restricted to short times after surface insertion.

1. Introduction

Turbulence near approximately flat shear-free gas–liquid interfaces occurs in a wide variety of environmental and industrial flows. This type of turbulence is often seen in rivers, lakes and ponds where it results from production by shear near the bottom wall or by unstable stratification. In engineering problems, it occurs in situations as different as heat film exchangers, open agitated vessels and tanks partially filled with liquid propellants, and it governs the large-scale dynamics of ship wakes. The structure of such a turbulence is the key to the understanding and prediction of heat and mass transfer rates across gas–liquid interfaces because most of the resistance to the transfer is generally located just below the interface,

owing to the respective values of the Prandtl/Schmidt numbers in both phases. This connection with heat and mass transfer problems has provided a strong motivation for clarifying the dynamical processes at work in the surface region and has led to many experimental and numerical investigations during the last two decades. From a more conceptual viewpoint, understanding the effect of a flat shear-free surface on an underlying homogeneous isotropic turbulence is a fundamental issue in turbulence modelling because any model aimed at predicting second-order turbulence statistics near impermeable surface should reproduce the essential features of this canonical situation.

Detailed experiments have established the major trends of the vertical distribution of the r.m.s. velocity fluctuations in open-channel flows (Komori *et al.* 1982; Nezu & Rodi 1986; Rashidi & Banerjee 1988) as well as in open water tanks where turbulence is produced by oscillating a grid vertically (McDougall 1979; Brumley & Jirka 1987). In both cases it has been shown that when the surface is approached, the vertical fluctuation is damped while the tangential ones are enhanced. In open-channel flows, the connection between the bursts generated near the bottom wall and the coherent motions which exist in the surface region and provide most of the 'renewal' of the surface has also been carefully studied (Nakagawa & Nezu 1977, 1981; Rashidi & Banerjee 1988; Komori, Murakami & Ueda 1989; Komori, Nagaosa & Murakami 1990). More recently, several investigations have focused on the detailed topology of the large-scale structures in the surface region (Rashidi 1997; Kumar, Gupta & Banerjee 1998).

Although much has been gained from these experiments, they have all suffered from the technical difficulties encountered in performing measurements very close to a deformable interface on which capillary ripples and contamination by surface-active materials can hardly be avoided. For that reason the determination of the r.m.s. velocities is not very accurate in the top few millimeters of the flow and many important quantities like vorticity fluctuations or dissipation have not yet been obtained. Moreover, as is usual in turbulent flows, statistical correlations involving pressure are beyond present experimental capabilities whereas they are of central importance to understanding how the surface affects the dynamics of the flow. To overcome these limitations, direct numerical simulation (DNS) has been extensively used during the last decade, mainly in the open-channel flow configuration. This technique has confirmed the experimental findings previously obtained and has produced detailed statistics throughout the flow as well as visualizations of the large-scale structures and their connection with bursting events (Lam & Banerjee 1992; Handler *et al.* 1993; Komori *et al.* 1993; Borue, Orszag & Staroselsky 1995; Handler *et al.* 1999). Some of these studies have also revealed some characteristics of the surface viscous sublayer in which the tangential vorticity components fall to zero in order to satisfy the shear-free boundary condition (e.g. Nagaosa 1999). They have also significantly contributed to describing the vorticity dynamics near the free surface (Leighton *et al.* 1991; Pan & Banerjee 1995) and the characteristics of the intercomponent transfer by which the energy of the vertical component is redistributed to the tangential ones (Swean *et al.* 1991, hereinafter referred to as SLHS; Handler *et al.* 1993; Komori *et al.* 1993; Nagaosa & Saito 1997; Nagaosa 1999).

The main limitation of all these numerical investigations is related to the smallness of the Reynolds number at which they can currently be performed. In the contributions mentioned above, Re^* (Reynolds number based on total depth and shear velocity at the bottom wall) ranges approximately from 130 to 250. Hence the surface-influenced region overlaps the logarithmic layer induced by the bottom

shear, with the consequence that the turbulent field 'seen' by the surface is strongly anisotropic. Furthermore these flow conditions imply that the thickness of the viscous sublayer attached to the free surface is a significant fraction (often more than 50%) of the integral length scale. Consequently it is difficult to disentangle viscous and inviscid processes near the surface at such Reynolds numbers. Compared to the canonical case of high-Reynolds-number isotropic turbulence interacting with a free surface, both aspects greatly complicate the fundamental understanding of dynamical processes intrinsically related to the presence of the surface.

The aim of the present investigation is to complete the picture provided by available low-Reynolds-number investigations by examining the near-surface results obtained in a high-Reynolds-number large-eddy simulation (LES) of an open-channel flow performed at a Reynolds number $Re^* = 1280$. Despite the well-known drawback of LES concerning the unresolved small scales, there are several advantages in exploring such data in detail. First, comparison of 'low-' and 'high-' Reynolds-number data may allow us to check or reveal the Re^*-scaling laws followed by the various statistical quantities. Second, as will be shown below, the anisotropy of the turbulence entering the surface-influenced region decreases significantly as Re^* increases. Consequently high-Reynolds number-data in which this underlying anisotropy is small shed light on the role played by the large anisotropy present in low-Reynolds-number situations. Third, we are particularly interested in checking the validity of the Hunt & Graham (1978, hereinafter referred to as HG) theory which was initially derived to describe the modification of second-order turbulence statistics after the sudden insertion of a flat surface in a high-Reynolds-number homogeneous isotropic turbulent field. Low-Reynolds-number DNS of decaying turbulence (Perot & Moin 1995) have suggested that this theory is only able to predict the very early stages of the flow. The situation simulated in our LES allows us to examine how the HG theory behaves at high Reynolds number in a statistically steady situation, i.e. after the flow has been influenced by the surface for a large number of turnover times.

To obtain reliable high-Reynolds-number LES data, we need a suitable subgrid-scale model in order to ensure that replacing DNS by LES will not produce significant artifacts in the large scales of the turbulent field. We have already employed the LES approach to study high-Schmidt-number mass transfer through the walls of a closed channel (Calmet & Magnaudet 1997, hereinafter referred to as CM). For that purpose the subgrid-scale stresses and scalar fluxes were closed using the dynamic mixed model (DMM) proposed by Zang, Street & Koseff (1993). Comparison of computational results with known turbulent statistics and well-established correlations for the mass transfer rate revealed a very good quantitative agreement, even with a modest discretization in the directions of homogeneity. Since turbulence distortion is less severe near a free surface than near a solid wall, there is no doubt that the LES approach using the DMM provides an accurate description of the large-scale dynamics in the surface-influenced region of an open-channel flow. This statement is supported by the detailed study of Salvetti *et al.* (1997) where free-surface decaying turbulence was studied using several different dynamic subgrid-scale models. In this study, the DMM emerged as one of the two models able to reproduce the characteristics of the decay process revealed by a reference DNS. As our goal in the present paper is to use LES as a reasonable generator of data and not to explore its possible refinements near a free surface, several computational aspects are deliberately ignored here. Such aspects include the possible optimization of the 'Leonard constant' of the subgrid-scale model (Salvetti & Banerjee 1995) or a systematic grid refinement study (we have carried out such a study in various configurations, starting from the grid used

in the present investigation, and did not find any significant effect on the statistics controlled by large-scale processes).

The plan of the paper is as follows. Section 2 describes the essential features of the computational approach used to obtain LES data (an extensive description of most of the technical aspects may be found in CM). Section 3 focuses on the comparison of low- and high-Reynolds-number r.m.s. velocity and vorticity statistics in the near-surface region, as obtained from the present LES and from available DNS. Similarly the high- and low-Reynolds-number energy balances and intercomponent energy transfer terms are compared in § 4 in order to obtain some insight into the nonlinear processes involved in the near-surface dynamics. Then a detailed comparison between the present LES results and predictions of the HG theory is reported in § 5. A summary and final remarks are given in § 6.

2. Computational aspects

2.1. *Numerical method*

As stated above, we generate high-Reynolds-number open-channel flow statistics by using the large-eddy simulation approach coupled with the dynamic mixed model proposed by Zang *et al.* (1993). The corresponding three-dimensional time-dependent equations are

$$\frac{\partial \overline{V}_i}{\partial x_i} = 0, \tag{1}$$

$$\frac{\partial \overline{V}_i}{\partial t} + \frac{\partial}{\partial x_j}(\overline{V}_i \overline{V}_j) = -\frac{1}{\rho}\frac{\partial \overline{P}}{\partial x_i} + \frac{\partial}{\partial x_j}[2(\nu + \nu_T)\overline{S}_{ij} - (\overline{\overline{V}_i \overline{V}_j} - \overline{\overline{V}}_i \overline{\overline{V}}_j)], \tag{2}$$

where $\overline{V}_i$ is the ith component of the resolved (or filtered) velocity field, $\overline{S}_{ij}$ denotes the resolved strain-rate tensor, and ρ and ν are the density and the kinematic viscosity of the fluid, respectively. The last term within round brackets in (2) is the so-called modified Leonard stress tensor (hereinafter denoted as L_{ij}) which can be explicitly obtained by re-filtering the resolved variable $\overline{V}_i$ and the products $\overline{V}_i \overline{V}_j$. Finally, the subgrid-scale viscosity $\nu_T = C_s \overline{\Delta}^2 |\overline{S}|$ is assumed to be proportional to the square of the local grid size $\overline{\Delta} = (\overline{\Delta}_1 \overline{\Delta}_2 \overline{\Delta}_3)^{1/3}$ and to the local strain rate $|\overline{S}| = (2\overline{S}_{ij}\overline{S}_{ij})^{1/2}$, $\overline{\Delta}_i$ being the local grid size in the ith direction. The way in which the parameter C_s is dynamically computed and locally re-filtered in order to remove possible negative values of the total viscosity $\nu + \nu_T$, the filtering procedures and other technical points are extensively described in Zang *et al.* (1993) and CM. The reader is also referred to these papers for a discussion of some interesting properties of the DMM, especially the importance of evaluating explicitly all components of the modified Leonard stress tensor, which contains the major part of the subgrid-scale energy.

The governing equations (1)–(2) are solved using the JADIM code already described by CM. Here we just recall that this code employs velocity and pressure as the primary variables and is based on a finite-volume approach in which all spatial derivatives are approximated with second-order centred schemes; temporal integration is achieved by means of a three-step Runge–Kutta/Crank–Nicolson algorithm. Incompressibility is satisfied at the end of the complete time step by solving a Poisson equation for an auxiliary potential from which the pressure $\overline{P}$ is deduced. The overall scheme is second-order accurate in both time and space. Validations of the code can be found in CM and in the references mentioned therein.

2.2. *Flow configuration and boundary conditions*

The physical situation considered in the present work consists of an open-channel flow of height 2δ in which turbulence is supposed to be fully developed (figure 1). The velocity field is assumed to be periodic along the streamwise (x) and spanwise (z) directions, the flow being driven by a constant streamwise pressure gradient $\mathrm{d}\mathscr{P}_0/\mathrm{d}x$. The overall momentum balance implies that this pressure gradient is directly related to the averaged shear stress ρu^{*2} at the bottom wall through

$$\frac{\mathrm{d}\mathscr{P}_0}{\mathrm{d}x} = -\frac{\rho u^{*2}}{2\delta}, \tag{3}$$

where u^* is the so-called friction velocity.

At the bottom wall ($y = 2\delta$) the fluid is subjected to the usual no-slip condition

$$U = V = W = 0, \tag{4a}$$

where U, V and W denote the instantaneous velocity components in the streamwise, vertical and spanwise directions, respectively. The upper boundary ($y = 0$) is modelled as a flat shear-free surface subjected to conditions

$$S_{12} = S_{23} = 0, \tag{4b}$$

$$V = 0, \tag{4c}$$

where S_{ij} is the unfiltered strain-rate tensor (throughout the paper subscripts 1, 2 and 3 correspond to directions x, y and z, respectively, see figure 1). Physically, conditions (4*b–c*) are appropriate for gas–liquid interfaces in situations where (*a*) velocity gradients in the gas are small (i.e. the motion in the liquid is not driven by the gas), (*b*) the liquid surface is free of impurities and surfactants, (*c*) surface tension and gravity are sufficiently strong to damp the vertical motions at the surface of the liquid, i.e. the Froude and Weber numbers are assumed to be negligibly small. To obtain the actual boundary conditions corresponding to the resolved velocity field, conditions (4*a–c*) must be filtered along the corresponding boundary. This yields

$$\overline{U} = \overline{V} = \overline{W} = 0 \quad \text{at} \quad y = 2\delta, \tag{5a}$$

$$\overline{S}_{12} = \overline{S}_{23} = 0 \quad \text{at} \quad y = 0, \tag{5b}$$

$$\overline{V} = 0 \quad \text{at} \quad y = 0. \tag{5c}$$

Conditions (5*a*)–(5*c*) complete the set of dynamical equations to be solved numerically. Placing condition (5*a*) into the expression for the subgrid stress tensor shows that the Leonard terms are identically zero at the bottom wall. Since the subgrid stress must vanish there for all i and j (because of conditions (4*a*) and (5*a*)) while several components of $\overline{S}_{ij}$ are non-zero, the subgrid-scale viscosity must vanish at the wall. As is now well established, this condition is automatically fulfilled by the values of C_s produced by the dynamic procedure (see e.g. Germano *et al.* 1991). At the upper surface, conditions (4*c*) and (5*c*) imply that the two off-diagonal components of the subgrid stress tensor involving the vertical direction ($i = 2$ or $j = 2$) must be zero. Injecting boundary conditions (5*b–c*) into the expression for the subgrid stress tensor shows that this requirement is satisfied even if the subgrid-scale viscosity keeps finite values at the surface. Consequently, there seems to be no particular difficulty in reproducing correctly the large-scale turbulent field in the free-surface region by means of the present LES approach.

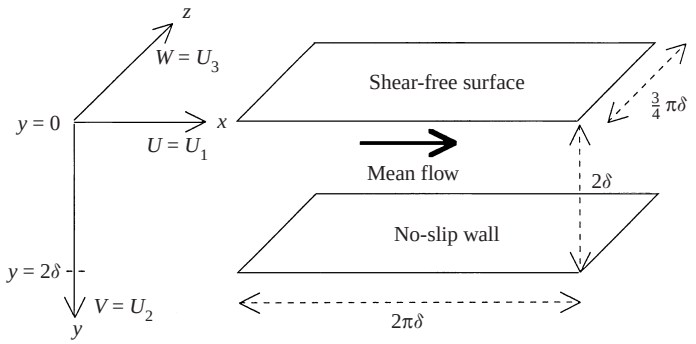

FIGURE 1. Coordinate system and computational domain.

2.3. *Computational runs*

In what follows we shall focus on LES results obtained at a single Reynolds number Re^*, based on the total depth 2δ and friction velocity u^*, equal to 1280. This value is selected because the LES study that we carried out previously in a plane channel flow (CM) was performed at $Re^* = 640$, based on the channel half-width δ. The latter choice suggests that, close to the lower wall, turbulence statistics will be very similar in both flows. Since these statistics were found to be in very good agreement with experimental data in CM, a similar agreement is expected here. Additionally, we can characterize quantitatively the degree to which the surface-influenced region and the bottom boundary layer interact by introducing the ratio δ/δ_w where δ_w is the characteristic thickness of the region entirely controlled by the solid wall. A rough estimate of δ_w is $30\nu/u^*$ which corresponds to the top of the buffer layer above the bottom wall. In the various DNS mentioned in § 1, the ratio δ/δ_w ranges from 2 to 4, suggesting that the integral length scale of the turbulent motions 'far' from the wall cannot be much larger than δ_w. In contrast, with $Re^* = 1280$ we obtain $\delta/\delta_w \approx 20$ and we can expect the existence of an intermediate region of the flow which is neither controlled by the bottom wall nor by the free surface. If so, many aspects of the dynamics of the near-surface region will be quite independent from the precise structure of the turbulence produced in the bottom boundary layer. In other words, this boundary layer will essentially play the role of a source of turbulence and it could be replaced by another type of source, like an oscillating grid for instance, without qualitatively affecting most of the statistical characteristics of the turbulence in the near-surface region.

Length scales in open-channel flows were studied by Handler *et al.* (1993) who showed in particular that for a given Reynolds number ($Re^* = 134$), the integral length scales in the homogeneous directions reach comparable maxima in an open channel and in a closed channel. In CM we computed a closed-channel flow with a computational domain $L_x \times L_y \times L_z = 2\pi\delta \times 2\delta \times 3\pi\delta/4$, the size of which was found to be convenient for obtaining small values of the two-point velocity correlations for separation distances of order $L_x/2$ or $L_z/2$. Based on the foregoing indications, we have maintained the previous values of L_x and L_z in the open-channel configuration. The $L_x \times L_z$ plane is discretized uniformly with 32 and 64 mesh points in the x- and z-directions respectively, yielding mesh spacings $\Delta x^+ \approx 125$ and $\Delta z^+ \approx 25$ in wall units. In CM, this computationally 'cheap' choice combined with the DMM was found to produce accurate statistics of near-wall turbulence. In the vertical direction, the grid spacing is determined by the requirement that at least three points lie in

the viscous sublayer attached to each boundary (see CM). Taking into account the foregoing considerations, 34 grid points are distributed in the lower half of the flow, i.e. between $y = \delta$ and $y = 2\delta$, following the geometrical transformation used in CM. This distribution yields a minimum grid spacing $\Delta y^+ = (u^*/\nu)\Delta y \approx 1$ near the lower wall. The determination of the minimum grid size required near the free surface is less straightforward because the thickness δ_V of the corresponding viscous sublayer is not very well known. Nevertheless, owing to the absence of shear, fewer small-scale structures are expected to be present near the free surface than near the bottom wall (Hunt (1984*a*). Hence it is reasonable to expect that the viscous sublayer near $y = 0$ is at least as thick as that near $y = 2\delta$. Consequently, most of the results presented below correspond to a grid where the points are distributed symmetrically with respect to the midplane $y = \delta$, i.e. 68 points are used in the vertical direction. Simulations have also been performed on a grid strongly refined in the upper part of the domain, yielding a minimum spacing $\Delta y^+ \approx 0.08$ just below the free surface, and a total number of 82 grid points in the vertical direction. This refinement does not improve the overall representation of the flow dynamics but it allows us to obtain statistics very close to the surface (see § 5).

Starting from an arbitrary turbulent field, integration was first performed until the statistics of the velocity field reached a nearly stationary state. In particular, it was checked that the mean shear stress had almost reached its linear equilibrium profile, so that (3) was satisfied. Then integration was pursued for several turnover times (typically five to ten) in order to obtain converged statistics of second-order quantities. In the following sections, the statistical quantities which are discussed result from averages performed in time as well as in the homogeneous directions x and z. For any variable Φ, $\langle\Phi\rangle$ denotes the corresponding average, φ'' is the resolved fluctuation with respect to this average (i.e. the resolved variable $\overline{\Phi}$ equals $\langle\overline{\Phi}\rangle + \varphi''$), and φ' is the total (i.e. resolved plus unresolved) fluctuation defined as $\varphi' = \Phi - \langle\Phi\rangle$.

3. High- and low-Reynolds-number velocity and vorticity statistics

In this section we first use the present LES results for r.m.s. velocity and vorticity fluctuations to determine the spatial extent of the various near-surface subregions of the flow. We also compare our high-Reynolds-number data with available low-Reynolds-number DNS results in order to clarify how near-surface r.m.s. velocity and vorticity statistics vary with the flow Reynolds number, i.e. to identify the relevant velocity and length scales near the surface. Available results in open-channel flows have generally been normalized using u^* and ν/u^* as in wall-bounded flows. Therefore, to keep the comparison with these results easy, we initially adopt the same normalization and use for instance the dimensionless distance $y_s^+ = yu^*/\nu$, which vanishes at the surface itself, to normalize near-surface quantities. However we shall see below that as the flow Reynolds number increases, the turbulence length scales become more and more independent of the viscous scale ν/u^* and another scaling must be selected.

3.1. *Velocity statistics*

Figure 2 shows the profiles of the r.m.s. intensities of the resolved turbulent fluctuations $v_1^+ = \langle v_i''^2\rangle^{1/2}/u^*$ (no summation on i) throughout the flow. Near the bottom wall the streamwise intensity u^+ reaches a maximum value about 3.0 as already found by CM; this maximum agrees well with the experimental value of 2.9 reported by Komori *et al.* (1989). More generally, the statistical characteristics observed close to the lower

wall are in good agreement with the DNS results reported by Borue *et al.* (1995). As the distance to the bottom wall increases, the anisotropy of the turbulence decreases. In the central region of the flow, say for $0.4 \leqslant y/\delta \leqslant 1$, the magnitudes of the vertical and spanwise intensities v^+ and w^+ are close to one another and the ratio u^+/w^+ is about 1.25 at $y/\delta = 0.5$. The free surface begins to damp the vertical velocity fluctuation at $y/\delta \approx 0.4$. This is the manifestation of the blocking effect due to the kinematic condition (4*c*). Closer to the surface, an increase of the tangential components is observed for $y/\delta \leqslant 0.15$. This behaviour has already been noticed in experiments (Komori *et al.* 1982; Rashidi & Banerjee 1988) as well as in computations (SLHS; Lam & Banerjee 1992; Komori *et al.* 1993; Borue *et al.* 1995; Nagaosa 1999; Handler *et al.* 1999), and will be discussed in more detail later. At the surface, figure 3 shows that u^+ reaches a maximum value of 0.91. This value lies in the range 0.8–1.2 of experimental data reported by Nezu & Rodi (1986) as well as in the range 0.85 (SLHS)–1.0 (Borue *et al.* 1995) of low-*Re* DNS results. The spanwise intensity also reaches a maximum value $w^+ \approx 0.82$ at the free surface. This value is close to the experimental result $w^+ \approx 0.75$ obtained by Komori *et al.* (1982) at $y/\delta \approx 0.2$ (no measurement was performed closer to the surface), and lies in the middle of the wide range 0.6 (SLHS)–1.05 (Komori *et al.* 1993) of previous DNS results. As pointed out in the introduction, detailed measurements are difficult to perform very close to a free surface and the uncertainty in r.m.s. velocity is quite large (Nezu & Rodi 1986). Similarly, spanwise velocities are quite sensitive to several aspects of the computations, like the size of the computational domain and the integration time (see in figure 2 the small undulations that remain on w^+ within the lower half of the flow). This probably explains why a significant dispersion exists in the results mentioned above. Taking into account this uncertainty, the foregoing results (including the present ones), suggest that the r.m.s. turbulent intensities measured in the free-surface region are only weakly sensitive to the flow Reynolds number. This is because dissipation is very small in the upper part of the flow (see below), so that for high enough Re^*, near-surface turbulent intensities do not decay significantly as the surface is approached. Using the above results for u^+ and w^+, we deduce that the r.m.s. value of the turbulent kinetic energy at the free surface is about $0.87u^*$ in the present high-Reynolds-number flow. This suggests that u^* can still be used as a characteristic scale of the velocity fluctuations in the near-surface region. In figure 3 we also notice that v^+ grows linearly with the distance to the surface in the subrange $0 \leqslant y_s^+ \leqslant 12$. This region, which is frequently referred to as the Kolmogorov sublayer (Brumley & Jirka 1988), corresponds to the zone of the flow where all the wavenumbers present in the vertical velocity spectrum are affected by the surface (see § 5). In this sublayer the normal strain rate $\partial v''/\partial y$ is constant and is determined, owing to continuity, by the value of the surface divergence $-(\partial u''/\partial x + \partial w''/\partial z)_{y=0}$ of the horizontal motions; hence the instantaneous flow is dominated by the existence of stagnation zones. This sublayer, the thickness of which will be confirmed later (see figure 7), is of crucial importance for estimating mass transfer rates in the high-Schmidt-number regime.

3.2. *Vorticity statistics and scaling laws*

Figure 4 shows profiles of the three r.m.s. resolvable vorticity fluctuations $\omega_1^+ = \langle \omega_1''^2 \rangle^{1/2} \nu/u^{*2}$ (no summation on i) in the vicinity of the free surface. Owing to conditions (5*b*) and (5*c*), the only vorticity component that can exist right at the surface is the vertical one, and this allows the existence of attached vortices and shear layers (Pan & Banerjee 1995; Nagaosa 1999). According to figure 4, all three components are almost constant and nearly equal to one another for $y_s^+ \geqslant 200$, and

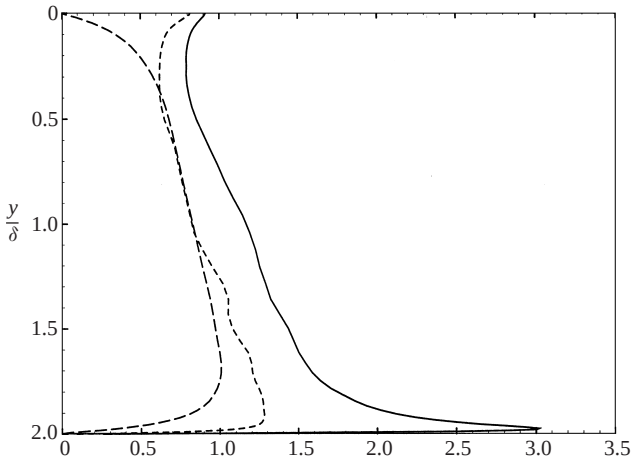

FIGURE 2. Resolvable turbulent intensities throughout the flow: ——, u^+; — —, v^+; – – –, w^+.

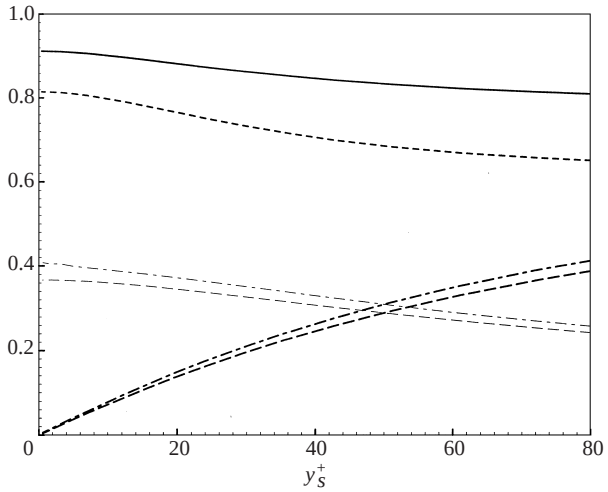

FIGURE 3. Resolvable turbulent intensities in the near-surface region: ——, u^+; — —, v^+; – – –, w^+; — · —, $(\langle v''^2\rangle + \langle L_{22}\rangle)^{1/2}/u^*$; ——, $50v^+/y_s^+$; ——— , $50(\langle v''^2\rangle + \langle L_{22}\rangle)^{1/2}/(u^* y_s^+)$.

this is still the case in the core of the flow (not shown). This is another indication that turbulence is not far from isotropy in this region. From $y_s^+ = 250$ to $y_s^+ = 25$, the vertical component ω_y^+ decreases gently whereas the tangential components increase by roughly the same amount. Combining the evolution of all three components reveals that the enstrophy $\sum_{i=1}^{3}(\omega_i^{+2})/2$ increases by about 20% between $y_s^+ = 250$ and $y_s^+ = 35$ where it exhibits a broad maximum. Then for $y_s^+ \leqslant 30$ (resp. $y_s^+ \leqslant 20$) ω_x^+ (resp. ω_z^+) falls to zero as required by the shear-free boundary condition, whereas the vertical fluctuation remains nearly unchanged. This behaviour, which is a key feature of free-surface turbulence (Sarpkaya 1996; Shen *et al.* 1999), provides a first estimate of the thickness δ_V of the viscous sublayer attached to the free surface. According to figure 4, $\delta_V^+ \approx 25$. We shall show in § 5.1 (see also figure 7) that after a suitable re-scaling this estimate agrees well with theoretical predictions (note that the Kolmogorov sublayer defined above is simply the top part of this viscous sublayer).

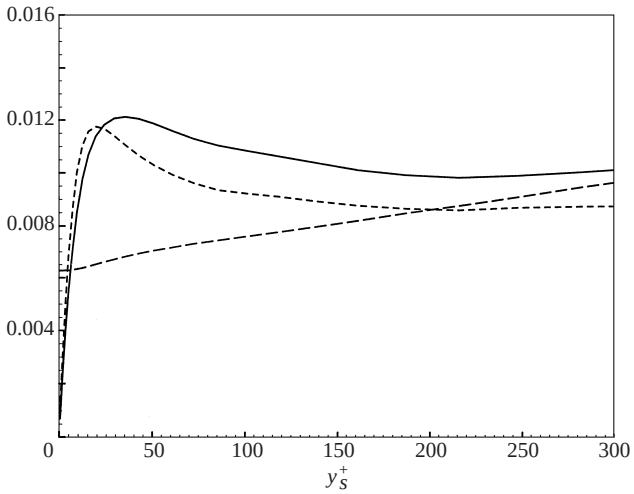

FIGURE 4. Resolvable vorticity fluctuations in the surface region: ——, ω_x^+; — —, ω_y^+; – – –, ω_z^+.

To compare near-surface values of the vorticity fluctuations found in the present high-Reynolds-number LES with those obtained in previous low-Reynolds-number DNS we must consider two points. First, as is usual in the LES approach, a significant part of the vorticity lies in the unresolved motions because the grid does not allow us to resolve small-scale velocity gradients. A quantitative estimate of the unresolved vorticity in the surface region can be obtained by using the well-known relation linking the enstrophy to the pseudo-dissipation $\langle\varepsilon'\rangle$, both quantities being defined using the total, i.e. resolved plus unresolved, fluctuations. Right at the free surface, this relation is, in the present flow, $\omega_y'^{+2} = \varepsilon'^{+} - \partial^2(v'^{+2})/\partial y_s^{+2}$ (Tennekes & Lumley 1972, p. 88), with $\omega_y'^{+} = (\nu/u^{*2})\langle\omega_y'^2\rangle^{1/2}$, $\varepsilon'^{+} = (\nu/u^{*4})\langle\varepsilon'\rangle$, and $v'^{+} = \langle v'^2\rangle^{1/2}/u^*$. Obviously the foregoing quantities cannot be determined exactly from LES. Nevertheless a good estimate of ε'^{+} can be obtained by computing the effective pseudo-dissipation ε_K involved in the LES; ε_K takes into account the effect of the subgrid-scale dissipation and can be determined from the turbulent kinetic energy balance (see below). Similarly, since most of the unresolved energy lies in the modified Leonard stress tensor (Zang *et al.* 1993; CM), a good estimate of v'^{+2} can be obtained by adding the resolved vertical energy v^{+2} and the corresponding averaged Leonard stress $\langle L_{22}\rangle$. In the vicinity of the surface this procedure yields $\varepsilon'^{+} \approx 3.0 \times 10^{-4}$ (see figure 5*b* below) and $v'^{+2} \approx 6.7 \times 10^{-5} y_s^{+2}$ (see figure 3). Hence we deduce that the actual surface value of the normal vorticity fluctuation is $\omega_y'^{+} \approx 1.3 \times 10^{-2}$, which is nearly twice as large as the resolved value shown in figure 4.

The second point to be considered in comparing low- and high-Reynolds-number vorticity statistics is the evolution of $\omega_i'^{+}$ with the flow Reynolds number, independently from the presence of the surface. In homogeneous isotropic turbulence, the typical magnitude of $\omega_y' = \partial u'/\partial z - \partial w'/\partial x$ is $\omega_y'^{+} \sim (u^+/L_\infty^+)(L_\infty^+/\lambda^+)$ where λ and L_∞ denote the Taylor microscale and the integral scale, respectively. Assuming that the usual scaling laws of isotropic turbulence hold locally in the present situation and noting that L_∞ is necessarily $O(\delta)$ (i.e. $L_\infty^+ = O(Re^*)$) because the largest scales are constrained by the total depth, one can expect $\omega_y'^{+}$ to evolve as $(u^+/L_\infty^+)Re^{*1/2}$ (Tennekes & Lumley 1972, p. 67). Then, since we saw that u^+ is $O(1)$ at the surface whatever Re^*, we conclude that $\omega_y'^{+}$ must be proportional to $Re^{*-1/2}$ near the surface.

Leighton *et al.* (1991) and Borue *et al.* (1995) found surface values of ω_y^+ equal to 0.035 ($Re^* = 134$) and 0.027 ($Re^* = 250$), respectively. Applying the proposed scaling law to their results yields a surface value of $\omega_y'^+$ about 1.2×10^{-2} for $Re^* = 1280$, a prediction which is indeed consistent with our previous estimate. Hence we conclude that owing to the relation between the magnitude of vorticity fluctuations and the flow Reynolds number, the surface vorticity varies with the Reynolds number when normalized by wall variables. This indicates that, while u^* is still a convenient velocity scale in the surface region (because the turbulent intensity is $O(u^*)$ whatever Re^*), ν/u^* is not the correct length scale to characterize near-surface vorticity and related quantities. The convenient scale is undoubtedly the Taylor microscale, which may be expressed in the form

$$\lambda/L_\infty = (L_\infty u^*/\nu)^{-1/2} \sim Re_\infty^{-1/2}, \tag{6}$$

where Re_∞ is the Reynolds number (to be defined in § 5.1) characterizing the turbulent field just below the surface-influenced region. Note that this evolution of the surface vorticity with the flow Reynolds number is not caused by the presence of the surface. It just expresses the fact that for large enough Reynolds number, the length scales of the turbulent field entering the near-surface region are independent of those that characterize the turbulence in the region where it is generated, i.e. near the bottom wall.

Let us now return to the viscous damping of ω_x^+ and ω_z^+. As pointed out above, this damping occurs in the viscous sublayer of thickness δ_V where the vertical gradient of the tangential velocities decreases in order to satisfy the condition (5*b*) at the surface, thus inducing a small change in these velocity components. The estimate $\delta_V/L_\infty = O(Re_\infty^{-1/2})$ (Hunt 1984*a*; Wu 1995) yields $\delta_V^+ = \delta_V u^*/\nu = O(Re^{*1/2})$. Using the near-surface evolution of ω_x^+ and ω_z^+ obtained by Leighton *et al.* (1991) and Borue *et al.* (1995), it turns out that $\delta_V^+ \approx 8$ for $Re^* = 134$ and $\delta_V^+ \approx 13$ for $Re^* = 250$. Therefrom, the foregoing scaling argument suggests that δ_V^+ should be between 25 and 30 for $Re^* = 1280$, in close agreement with the estimate obtained directly from figure 4. Comparing with the previous discussion we see that for physical reasons of different origin, δ_V and the near-surface value of ω_y^+ obey the same Re^*-scaling law.

4. Mechanisms governing the energy transport and the intercomponent energy transfer

Here we use again our high-*Re* LES statistics and some of the available low-*Re* DNS data to analyse the near-surface evolution of the various terms involved in the budget of the turbulent kinetic energy and that of the diagonal components of the pressure–strain correlation tensor. This comparison between high- and low-Reynolds-number results appears to be useful to disentangle viscous and inviscid processes and to shed light on the influence of the anisotropy of the bulk turbulence on the intercomponent energy transfer mechanisms.

4.1. *Turbulent kinetic energy balance*

Taking into account the statistical stationarity of the turbulent field as well as its homogeneity in the x- and z-directions, the resolvable turbulent kinetic energy (TKE) budget can be written in the form

$$0 = -\varepsilon_K - \langle u''v''\rangle \frac{\partial \langle \overline{U} \rangle}{\partial y} - \frac{\partial}{\partial y}\left[\langle \mathscr{K} v''\rangle + \frac{1}{\rho}\langle p''v''\rangle + \langle L_{i2} v_i''\rangle - \langle \nu + \nu_T\rangle \frac{\partial K}{\partial y}\right], \tag{7}$$

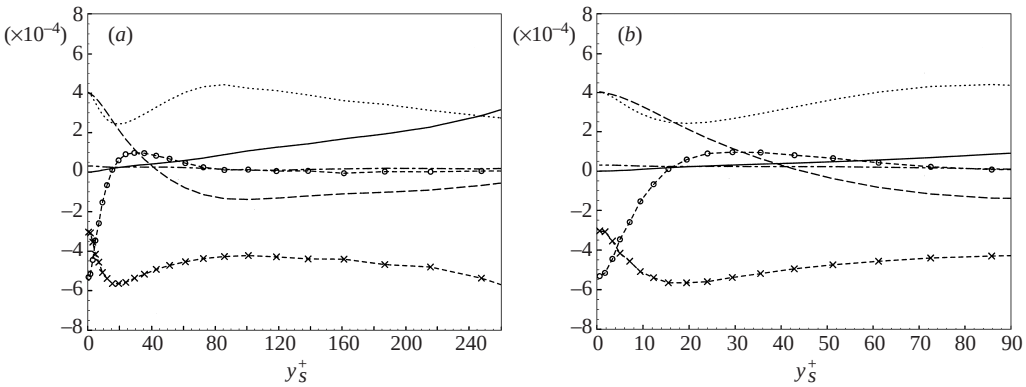

FIGURE 5. Terms of the resolvable turbulent kinetic energy balance: (*a*) throughout the surface-influenced region $y/\delta \leqslant 0.4$; and (*b*) close to the surface ($y/\delta \leqslant 0.15$). All terms are normalized by ν/u^{*4}. ——, production P_K; ·····, turbulent transport T_K; — —, pressure-diffusion Π_K; — — —, cascade term TL_K; ○–○, diffusion D_K; ×–×, pseudo-dissipation ε_K.

where $\mathscr{K} = (u''^2 + v''^2 + w''^2)/2$ and $K = \langle \mathscr{K} \rangle$. Owing to the splitting of velocity fluctuations into resolved and unresolved contributions, the exact definition of the pseudo-dissipation rate ε_K is rather complicated because it contains the expected positive contribution $\langle (\nu + \nu_T)(\partial v_i''/\partial x_k)^2 \rangle$ (with summation on i and k), plus subgrid-scale contributions of minor importance (see Moin & Kim 1982 and CM). The other terms in (7) correspond respectively to production by the mean shear (P_K), transport of turbulence by resolvable velocity fluctuations (T_K), pressure diffusion (Π_K), turbulent transport associated with the Leonard stresses (TL_K) (this term is often referred to as the 'cascade' term), and 'viscous' diffusion (D_K). Profiles of the various terms in the near-surface region are plotted in figure 5(a, b). The evolutions observed in these figures are more subtle than those encountered near a rigid wall because the boundary conditions (5*b–c*) allow all terms of (7) but P_K to be non-zero at the free surface as can be readily shown by expanding the velocity and pressure fluctuations in y_s^+-Taylor series (see SLHS). Note that using the governing equations (1)–(2), these Taylor expansions also show that all terms in (7) have a zero derivative at the free surface, as confirmed by figure 5(*b*). Production is clearly weak throughout the near-surface region: while P_K and T_K are nearly equal for $y_s^+ = 240$, the evolution of the turbulent energy closer to the surface, say for $y_s^+ \leqslant 100$, results essentially from a balance between the total diffusion term $T_K + \Pi_K + D_K$ and dissipation. The cascade term TL_K is negligible, whereas it is responsible for about 30% of the turbulent transport close to the bottom wall (see CM). This difference reflects the fact that there is a much smaller proportion of small-scale structures near the free surface than near the bottom wall, owing to the weakness of the mean shear in the upper part of the flow. The turbulent transport term T_K is positive everywhere and brings turbulent energy towards the surface. Far enough from the surface, say for $y_s^+ \geqslant 40$, D_K is negligible. In the same region, the pressure-diffusion term Π_K is negative and reduces the net transport of turbulence towards the surface.

According to figure 5(*b*), most terms of (7) vary much more rapidly with y_s^+ when $y_s^+ \leqslant 25$ than at larger distances from the free surface. This is because variations observed for $y_s^+ \leqslant 25$ correspond to viscous mechanisms whereas those observed at larger distances are driven by inviscid processes. The only exception is the pressure-diffusion term Π_K which experiences a mild variation everywhere. A typical example

of viscous process is provided by the evolution of D_K for $y_s^+ \leqslant 25$. Viscous diffusion becomes negative because the curvature of the TKE is negative at the surface, a direct consequence of the increase of the TKE in the near-surface region and of the boundary conditions (5*b–c*) that force the normal derivative of the TKE to vanish at the surface. Despite a significant reduction of ε_K very close to the surface, this behaviour of D_K produces a net increase of the sink terms in the TKE balance. This increase is balanced by Π_K which reaches a surface value of the same order as that of T_K. The sharp decrease of ε_K observed in the region $y_s^+ \leqslant 15$ was also noticed by Handler *et al.* (1993), Perot & Moin (1995), Walker, Leighton & Garza-Rios (1996), and Shen *et al.* (1999). Figure 5(*b*) indicates that ε_K is about 40% smaller at the surface than at $y_s^+ = 30$ (i.e. outside the viscous sublayer); this reduction agrees quantitatively with that found by Walker *et al.* (1996) who studied the long-time behaviour of freely decaying turbulence in presence of a free surface. Perot & Moin (1995) argued that this reduction of ε_K within the viscous sublayer results from a lack of the usual cascade mechanism, owing to the turbulent field right at the surface having only two components. Connections between free-surface turbulence and two-dimensional turbulence have also been evoked in some other investigations (Pan & Banerjee 1995; Kumar *et al.* 1998). However it was clearly established by Walker *et al.* (1996) that, even though $v', \partial u'/\partial y$ and $\partial w'/\partial y$ are zero at the surface, turbulence remains fully three-dimensional everywhere because the vertical gradient $\partial v'/\partial y$ is non-zero and provides the required strain rate for producing vertical vorticity through the usual vortex stretching mechanism (see also Shen *et al.* 1999 and Nagaosa 1999). In their recent extension of the HG thoery to the viscous sublayer, Teixeira & Belcher (2000) found (by comparison with DNS) that rapid distortion theory predicts correctly the short-time evolution of the dissipation profile up to the surface. They pointed out that this successful prediction indicates that the near-surface dissipation profile is not a result of small-scale processes; rather it is determined by the vertical gradients of the large-scale motions subjected to the viscous damping associated with the free-surface condition (5*b*). The present results strongly support this statement and extend it to longer times, since comparison with the DNS of Walker *et al.* (1996) suggests that the dissipation profile is well predicted by the LES, which does not describe in detail most of the small-scale dynamics in the directions of homogeneity.

The TKE budget was also analysed by SLHS and Handler *et al.* (1993) for $Re^* = 134$. The corresponding results are qualitatively similar to those discussed above. They show in particular that T_K is positive throughout the surface layer, that Π_K (resp. D_K) becomes positive (resp. negative) close to the surface, and they exhibit the aforementioned reduction of ε_K at the free surface. In line with our discussion concerning the relevant length scales in the surface layer, these results cannot be compared quantitatively with the present ones when expressed in 'wall' units. According to our previous conclusions, such a comparison requires that distances be multiplied by $Re^{*-1/2}$ in the viscous sublayer ($y \leqslant \delta_V$) and by Re^{*-1} below it because the relevant length scale is L_∞ in the inviscid part of the surface-influenced layer. Similarly, any term of (7) previously normalized by u^{*4}/ν must be multiplied by Re^* because ε_K scales with the enstrophy, and so does the whole diffusion term $T_K + \Pi_K + D_K$. It must however be noticed that D_K is a viscous contribution which depends also on Re^*; consequently T_K and Π_K may also exhibit some Re^*-dependence as will be shown below. Since the Reynolds number of our LES is nearly ten times larger than that of SLHS, this re-scaling suggests that the terms of (7) plotted in figure 5(*b*) should be one order of magnitude smaller than theirs, while the typical length over which any variation of these terms occurs in the range $y_s^+ \leqslant 25$ should be about

three times larger. This statement can be easily confirmed. For instance in figure 9 of SLHS one observes that the decrease of D_K (resp. ε_K) towards its surface value takes place over roughly eight (resp. six) 'wall' units whereas our figure 5(b) shows that the same trend starts around $y_s^+ = 25$ (resp. $y_x^+ = 16$). Similarly SLHS found a surface value of the pseudo-dissipation of about 3.2×10^{-3} whereas the corresponding value is about 3.0×10^{-4} in figure 5(a). In contrast, their surface value of D_K is only three times larger than that of figure 5(a) and hence their surface values of T_K and Π_K are only six times larger than those of our LES. As suggested previously, this is a low-Reynolds-number effect related to the dependence of D_K on Re^*; since the increase of the TKE as the surface is approached is much smaller when Re^* is small (as confirmed by the vertical profile of the TKE in figure 2 of SLHS), this results in smaller surface values of $\partial^2 K/\partial y^2$ and D_K.

4.2. *Pressure–strain correlations*

To save space we do not comment on the budget of the individual components of the resolvable Reynolds stress tensor. However, it is of great interest to describe the evolution of the diagonal components of the resolvable pressure–strain correlation tensor $\phi_{ij} = 2(u^{*4}/\nu)\langle \overline{P}\,\overline{S_{ij}} \rangle$ that governs energy transfer between the three components of the resolvable turbulent energy. This evolution is shown in figure 6 in the region $y_s^+ \leqslant 180$, i.e. $y/\delta \leqslant 0.28$. In the absence of any boundary, the usual role of the pressure–strain term is to reduce the anisotropy that may exist in the turbulent field (mechanism I). However, it has been recognized for a long time that the presence of an impermeable boundary affects not only the normal r.m.s. velocity but also the tangential components of the turbulent energy. The most common interpretation of this phenomenon is that energy is transferred from the normal component to the tangential ones through pressure–strain correlations (Launder, Reece & Rodi 1975; Gibson & Launder 1978). Such a mechanism suggests that in the presence of a boundary, ϕ_{ij} tends to increase the local anisotropy rather than to decrease it (mechanism II). Throughout the region shown in figure 6 we have $\langle u''^2 \rangle > \langle w''^2 \rangle > \langle v''^2 \rangle$ (see figure 2). According to figure 6, ϕ_{22} is negative for $y_s^+ \leqslant 80$, indicating that near the surface v^+ transfers energy towards both tangential r.m.s. fluctuations, and this corresponds indeed to mechanism II. Only far enough from the surface ($y_s^+ \geqslant 80$) is the isotropization process observed; there ϕ_{11} is negative, so that the largest turbulent intensity u^+ transfers energy towards v^+ and w^+. Very close to the surface one notices that the spanwise component receives slightly more energy than the streamwise one. This trend was also observed by SLHS, Komori *et al.* (1993) and Nagaosa (1999). However the difference $\phi_{33} - \phi_{11}$ is much larger in these low-Reynolds-number DNS, and this results in a much larger increase of w^+ compared to u^+ near the free surface.

In order to disentangle the processes affecting ϕ_{ij}, we compare our results with those of SLHS. For this purpose we apply the re-scaling laws derived above, keeping in mind that ϕ_{ij} scales with dissipation at high Reynolds number, i.e. it must be proportional to Re^{*-1}. We find that the surface value of ϕ_{33} determined by the previous authors is ten times that found in figure 6. Similarly, the distance between the location at which ϕ_{33} reaches a minimum and the outer edge of the viscous sublayer ($y = \delta_V$) is ten times larger in figure 6 than in the corresponding plot of SLHS. These results clearly indicate that ϕ_{33} is essentially governed by the inviscid processes related to the blocking effect rather than by viscous processes due to the viscous sublayer. When the same procedure is applied to ϕ_{11} it reveals very different behaviours. For instance, the surface value of ϕ_{11} found by SLHS is about three times that found in figure 6. Similarly the location at which ϕ_{11} becomes positive in

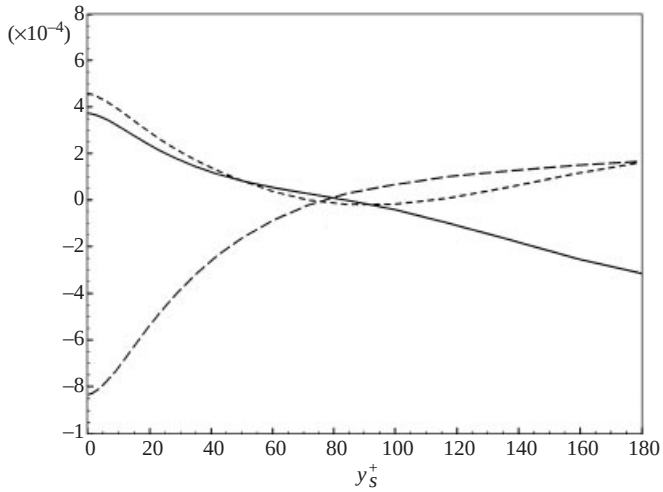

FIGURE 6. Resolvable presure–strain correlations near the surface (all terms are normalized by ν/u^{*4}: ——, ϕ_{11}; — —, ϕ_{22}; – – –, ϕ_{33}).

the low-Reynolds-number DNS lies within the viscous sublayer whereas this change of sign arises much farther from the surface ($y_s^+ \approx 85$) in the high-Reynolds-number case. At first glance these differences could be attributed to near-surface viscous effects. However, if turbulence were perfectly axisymmetrical about the y-axis, the evolution of u'' and w'' would be identical, irrespective of viscous effects, and so would be that of ϕ_{11} and ϕ_{33}. Hence it is likely that the differences observed between high- and low-Reynolds-number behaviours originate in the horizontal anisotropy of the turbulence entering the surface-influenced region. In the DNS of SLHS the free surface begins to affect turbulent intensities at a distance from the bottom wall $(2\delta - y)u^*/\nu$ about 95. At such a distance, the bottom wall still controls the local structure of the turbulent field almost entirely and the anisotropy of the large-scale motions is large. More precisely, at this location SLHS data indicate $u^{+2}/K^+ \approx 1.15$, $v^{+2}/K^+ \approx 0.30$, $w^{+2}/K^+ \approx 0.55$, with $K^+ = K/u^{*2}$. At the same normalized distance from the bottom wall (corresponding to $y/\delta = 1.85$ in figure 2), our LES data yield $u^{+2}/K^+ \approx 1.16$, $v^{+2}/K^+ \approx 0.30$, $w^{+2}/K^+ \approx 0.54$, confirming that turbulent intensities scale completely with ν/u^*, i.e. with wall variables. In our high-Reynolds-number flow, figure 2 indicates that turbulence intensities begin to be affected by the free surface at $y/\delta \approx 0.4$, a location where $u^{+2}/K^+ \approx 0.89$, $v^{+2}/K^+ \approx 0.57$, $w^{+2}/K^+ \approx 0.54$. These values are much closer to isotropy than those of SLHS, confirming that the anisotropy of the turbulence entering the surface region decreases significantly as the flow Reynolds number increases. Then the origin of the differences between SLHS data for ϕ_{11} (and ϕ_{22} by virtue of continuity) and the present LES results becomes clear. Whatever the Reynolds number, mechanism II acts in the surface layer, that is v^+ transfers energy towards u^+ and w^+. However, at low Reynolds number the streamwise fluctuation entering the surface layer is much larger than the other two. Hence mechanism I acts through most of this layer to reduce this outer anisotropy, that is u^+ transfers energy towards v^+ and w^+. Combining both processes shows that mechanisms I and II act together to bring energy to the spanwise fluctuation. This explains why the increase of w^+ close to the free surface is much larger than that of u^+ in the low-Reynolds-number case. In contrast, at large Reynolds number, mechanism I acts secondarily since the outer anisotropy is moderate, and the entire

surface layer is dominated by mechanism II. In figure 6 ϕ_{11} and ϕ_{33} are seen to have similar magnitudes throughout a large part of the surface layer (roughly $y_s^+ \leqslant 80$), indicating that the high-Reynolds-number flow simulated in our LES is fairly close to an 'ideal' flow where turbulence would be axisymmetrical about the vertical axis. To summarize, we may say that inside the surface-influenced layer, $\phi_{ij}(y)$ scales with the anisotropy tensor $A_{ij} = \langle v_i'' v_j'' \rangle / K - (2/3)\delta_{ij}$ (δ_{ij} being the Kronecker tensor) evaluated at the bottom of the surface layer, and with the relevant dimensionless distance, i.e. $(y - \delta_V)/L_\infty$ if $y \geqslant \delta_V$ or y/δ_V if $y < \delta_V$. This argument is consistent with the fact that, having noticed similar values of w^{+2}/K^+ in the present LES and in the DNS of SLHS at the bottom of the surface-influenced layer, we observe identical evolutions of ϕ_{33} throughout it.

5. Comparison of LES results with predictions of the HG theory

As stated in the introduction, a theory based on the rapid distortion approximation was elaborated by HG to describe the modifications induced by the sudden insertion of a flat impermeable surface to the second-order turbulent moments of an initially homogeneous isotropic turbulence. Given its basic assumptions, it is generally supposed that this theory is valid only for short time after surface insertion. While low-Reynolds-number DNS performed by Perot & Moin (1995) reinforce this suspicion, several experiments in which the turbulence is statistically steady suggest that the HG theory may be valid even at long time. It is the purpose of this section to reconsider this point by comparing the high-Reynolds-number LES results with some of the most significant predictions of the HG theory, especially those concerning the evolution of the integral length scales, one-dimensional velocity spectra and r.m.s. velocity fluctuations throughout the so-called source layer, i.e. the almost inviscid part of the surface-influenced layer.

5.1. *Global characteristics of the surface-influenced layer*

To compare LES data with predictions from the HG theory, we first need to determine the integral length scale L_∞ and the velocity scale $\mathscr{u}$ that characterize the turbulent field just below the surface-influenced layer. This will allow us to evaluate the thickness of the various subregions of the surface-influenced layer and the changes of the r.m.s. velocity fluctuations throughout these subregions in terms of the turbulent Reynolds number.

The length scale L_∞ may easily be obtained using Taylor's estimate $\varepsilon_K \sim \mathscr{u}^3/\ell$ (Batchelor 1953, p. 103), since the turbulent macroscale ℓ is just $2L_\infty$ in isotropic turbulence (Tennekes & Lumley 1972, p. 273). Using the isotropic relation $\mathscr{u}^3 = (2K/3)^{3/2}$, we deduce L_∞ from the profile of the quantity $(2K/3)^{3/2}/(2\varepsilon_K)$ plotted through the central part of the flow: this procedure shows a clear plateau at 0.40δ. This value indeed corresponds to the location beyond which velocity fluctuations v^+ and w^+ plotted in figure 2 follow separate evolutions. Hence this result confirms the prediction of HG that the surface affects the flow field over a surface-influenced region (or surface layer) whose typical thickness is L_∞ (figure 7). The above value of L_∞ may be confirmed by considering the low-wavenumber part of the longitudinal spectrum of the streamwise velocity $E_u(k_x)$ at $y_s^+ = 180$ (figure 8 below), a location where near-surface effects are still small. Therefrom, the general relation between longitudinal spectra and integral length scales $E_i(k_x \to 0) = \langle v_i''^2 \rangle {}^xL_i/\pi$ (Tennekes & Lumley 1972, p. 273) yields $L_\infty = {}^xL_u \approx 0.39\delta$, ${}^xL_u$ denoting the longitudinal integral scale. In addition we notice that at the same location the longitudinal spectrum of the

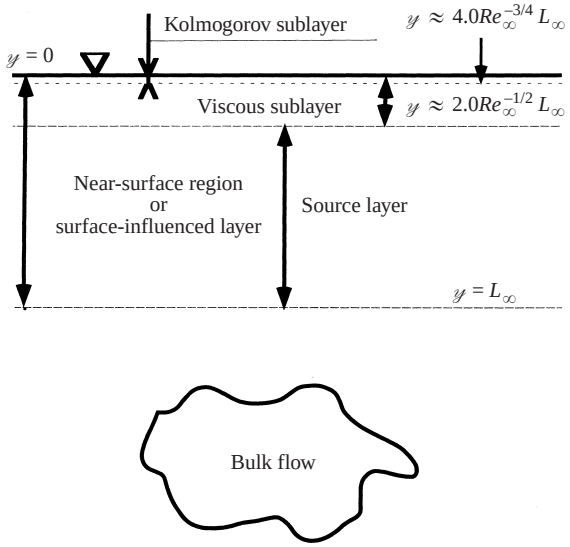

FIGURE 7. Structure of the surface-influenced layer.

spanwise velocity $E_w(k_x)$ yields ${}^xL_w \approx 0.23\delta$. Hence the isotropic relation ${}^xL_w = {}^xL_u/2$ is approximately satisfied. Using the above value of L_∞ and the value of K at $y \approx L_\infty$, we deduce that the turbulent Reynolds number $Re_\infty = \mathscr{u}\ell/\nu$ characterizing the turbulence below the surface-influenced region is about 360.

We can now re-evaluate the thickness of the various subregions of the surface-influenced layer in terms of the turbulent Reynolds number (figure 7). The thickness of the viscous sublayer is obtained by using the estimate $\delta_V^+ \approx 25$ deduced from figure 4. This yields $\delta_V/L_\infty = \delta_V^+(Re^* L_\infty/\delta)^{-1} \approx 0.098$. Hunt (1984*a*) pointed out that δ_V/L_∞ must scale with $Re_\infty^{-1/2}$, and measurements by Brumley & Jirka (1987) indicated $\delta_V/L_\infty \approx 2.0Re_\infty^{-1/2}$. Our estimate of δ_V/L_∞ agrees well with this finding, since the above value, $Re_\infty = 360$, yields $2.0Re_\infty^{-1/2} \approx 0.105$. Hence we conclude that in our high-Reynolds-number LES, the thickness of the viscous sublayer is typically one-tenth of L_∞. The thickness δ_K of the Kolmogorov sublayer detected in figure 3 can also be evaluated (figure 7). For isotropic turbulence, the Kolmogorov microscale η_K is estimated to be $2.0Re_\infty^{-3/4}L_\infty$ (Brumley & Jirka 1988). In the present high-Reynolds-number flow this yields $\eta_K/L_\infty \approx 2.4 \times 10^{-2}$, and figure 3 suggests $\delta_K/L_\infty \approx 4.7 \times 10^{-2}$, i.e. $\delta_K \approx 2.0\eta_K$ or equivalently $\delta_K/L_\infty \approx 4.0Re_\infty^{-3/4}$.

Within the Kolmogorov sublayer we may write $v'' \approx y(\partial v''/\partial y)$ or equivalently, $v^+ = O(\varepsilon_K^{+1/2})y_s^+ = O(Re_\infty^{-1})y_s^+$ according to the scaling laws discussed in § 3.2. Then, since $\eta_K^+ = O(Re_\infty^{1/4})$ (Monin & Yaglom 1975, p. 349), integration of v^+ across the Kolmogorov sublayer yields the r.m.s. vertical velocity fluctuation $(\Delta v)_K$ at $y = \delta_K$ as

$$(\Delta v)_K/\mathscr{u} = O(Re_\infty^{-1/4}). \tag{8a}$$

Hence, for turbulent Reynolds numbers of some hundreds, 20% to 30% of the total variation of the vertical fluctuation in the surface-influenced region takes place within the Kolmogorov sublayer. The variation $(\Delta\mathscr{u})_V$ of the tangential r.m.s. velocities across the viscous sublayer shown in figure 7 can also be estimated by the following argument. Within the viscous sublayer $\partial v''/\partial x$ is much smaller than $\partial u''/\partial y$. This implies $\omega_z'' \approx -\partial u''/\partial y$, so that we can write $\partial\langle u''^2\rangle/\partial y \approx -2\langle u''\omega_z''\rangle$. Integrating this relation

across the viscous sublayer yields $\mathscr{u}(\Delta\mathscr{u}U)_V = O(\langle u''\omega_z''\rangle\delta_V) = O(\langle u''\omega_z''\rangle L_\infty Re_\infty^{-1/2})$. To estimate the correlation $\langle u''\omega_z''\rangle$, care must be taken that the characteristic length scales of velocity and vorticity fluctuations are different, since u'' may be characterized by scales of $O(L_\infty)$, whereas ω_z'' is characterized by scales of $O(\lambda)$, λ being the Taylor microscale. Assuming that this weak overlap in spectral space decreases the correlation between u'' and ω_z'' by a factor proportional to the scale ratio λ/L_∞ (Tennekes & Lumley 1972, p. 81) yields $\langle u''\omega_z''\rangle = O(\mathscr{u}\ \mathscr{u}/\lambda\ \lambda/L_\infty) = O(\mathscr{u}^2/L_\infty)$, from which we deduce

$$(\Delta\mathscr{u})_V/\mathscr{u} = O(\mathrm{Re}_\infty^{-1/2}). \tag{8b}$$

According to this estimate, $(\Delta\mathscr{u})_V/\mathscr{u}$ should be about 5% for $Re_\infty = 360$, a prediction confirmed by the r.m.s. velocity profiles of figure 3.

5.2. *Spectra and variances*

One-dimensional velocity spectra are plotted in figure 8 for various distances to the free surface. Only the low-wavenumber range (typically $k_x\delta \leqslant 8$) is meaningful in these spectra, owing to the coarse mesh used in the streamwise direction. Moreover the minimum resolvable wavelength is $2\pi\delta/16 \approx 0.39\delta$ which is of the same order as L_∞. Hence effects affecting wavenumbers larger than $2\pi L_\infty^{-1}$ are not resolved. Despite these limitations, figure 8 gives interesting information which is more easily discussed by introducing the normalized distance $Y_S = (y - \delta_V)/(L_\infty - \delta_V)$; with this definition, the range $0 < Y_S < 1$ corresponds to the 'source' layer of the HG theory (see figure 7), i.e. to the part of the surface-influenced region where viscous effects are negligible (note that instead of Y_S, HG defined the dimensionless length scale $Y = y/L_\infty$ because they assumed that δ_V/L_∞ was negligibly small). Figures 8(a) and 8(c) show that for $0 < Y_S < 1$ the low-wavenumber part of the streamwise spectrum $E_u(k_x)$ is almost unaffected by the distance to the surface while the energy corresponding to $k_x\delta = 1$ in the spanwise spectrum $E_w(k_x)$ increases as the surface is approached: at $y_s^+ = 21$ which is close to $Y_S = 0$, $E_w(k_x\delta = 1)$ is 2.5 times larger than at $y_s^+ = 180$ and the ratio $E_u(k_x\delta = 1)/E_w(k_x\delta = 1)$ reaches the value 1.03. These trends are consistent with the HG theory which predicts that in the limit $k_xL_\infty \to 0$, $E_u(k_x)$ remains unchanged as $Y_S \to 0$ while $E_w(k_x)$ increases by a factor of 2, so that the ratio E_u/E_w becomes unity at $Y_S = 0$. Using the values of u^+ and w^+ corresponding to $y_s^+ = 21$ (figure 3), the evolution of the streamwise and spanwise integral length scales across the source layer can also be obtained. This yields ${}^xL_u(Y_S \to 0) \approx 0.80L_\infty$ and ${}^xL_w(Y_S \to 0) \approx 0.96L_\infty$, which shows that the streamwise (resp. spanwise) integral scale is reduced (resp. increased) as the surface is approached. This is also consistent with the theory, which for isotropic turbulence predicts ${}^xL_u = {}^xL_w = (2/3)L_\infty$ for $Y_S \to 0$. Most of the quantitative differences remaining between the LES results and the theoretical predictions may probably be explained by the finite thickness of the viscous sublayer which limits the amplification of the tangential velocities slightly below the theoretical prediction, and by the anisotropy of the turbulence entering the surface region which is not accounted for by the theory.

The most spectacular influence of the surface is of course found in the v''-spectrum. As the surface is approached, all wavenumber components of the v''-spectrum resolved by the computational grid are progressively damped, owing to the blocking of the large eddies by the surface. A similar evolution was reported in the experiments of Thomas & Hancock (1977), Brumley & Jirka (1987) and Hannoun, Fernando & List (1988), as well as in the DNS studies of Handler *et al.* (1993) and Pan & Banerjee (1995). Note, however, that moderate-to-high wavenumber components (typically

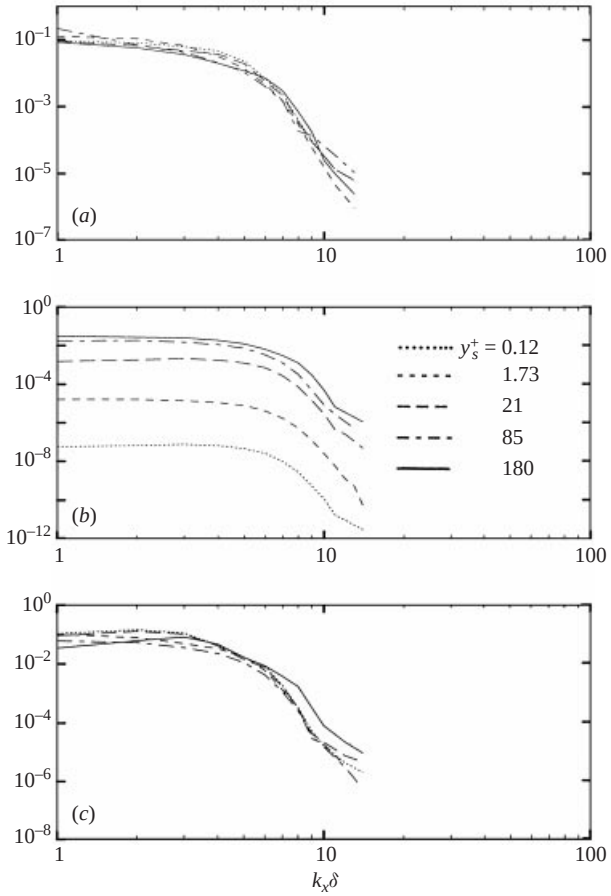

FIGURE 8. One-dimensional velocity spectra in the surface-influenced region: (*a*) u''; (*b*) v''; (*c*) w''.

$k_x > (L_\infty Y_S)^{-1}$) that are not resolved in the present LES (nor in previous 'DNS', see Handler *et al.* (1993)) are not blocked by the surface, so that the spectral density of $E_v(k_x)$ is unaltered at such wavenumbers in the aforementioned experiments. Within the source layer, the HG theory predicts that in the low-wavenumber range $k_x Y_S \ll 1$, the v'-spectrum obeys the law $E_v(k_x) = \gamma \varepsilon_\infty^{2/3} (L_\infty Y_S)^{5/3}$ with $\gamma = 1.125$ (Hunt 1984*b*), ε_∞ being the dissipation rate of the free-stream turbulence. To check this prediction, we replace ε_∞ by the average value ε_{Kav} of ε_K in the layer $0 < Y_S < 0.7$ ($\varepsilon^+_{Kav} \approx 4.5 \times 10^{-4}$ according to figure 5*a*) because it can be shown that at leading order the distortion of the flow in the source layer does not alter the dissipation rate (see Teixeira & Belcher 2000; Magnaudet 2003). Evaluating the product $E_v(k_x)\varepsilon_{Kav}^{-2/3}(L_\infty Y_S)^{-5/3}$ then shows that the $Y_S^{5/3}$ scaling law is supported well by the numerical results. The value of this product, i.e. γ, is found to fluctuate slightly in the range 1.0–1.2, the fluctuations being probably due to the marginally convenient statistical sampling and to the underlying inhomogeneity of the flow not accounted for by the theory. The essential consequence of the above scaling law is that the r.m.s. vertical velocity evolves as $Y_S^{1/3}$ in the source layer. Figure 9 shows the evolution of v^{+3} for $y \leqslant L_\infty$. Outside the viscous sublayer, this evolution is almost perfectly linear up to $Y_S = 0.7$, thus confirming the $Y_S^{1/3}$ scaling. Note that the linear fit shown in figure 9 suggests a virtual origin of

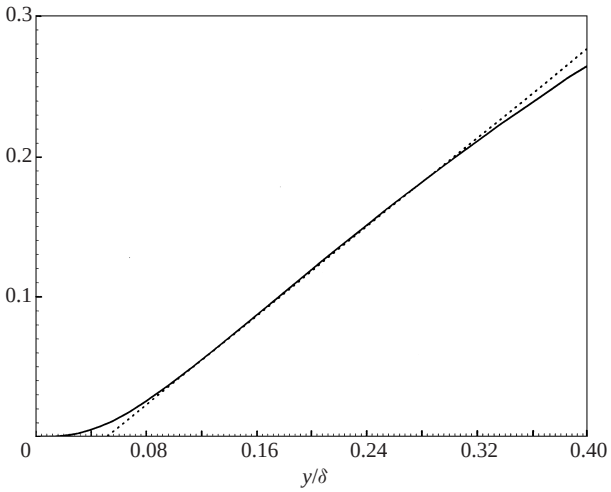

FIGURE 9. Evolution of the normal velocity fluctuation in the surface region: ——, v^{+3}; - - - - -, $v^{+3} \propto y/\delta$.

the source layer located at $y/\delta \approx 0.05$, thus emphasizing the existence of the viscous sublayer. Theoretical integration of the v'-spectrum yields $\langle v'^2 \rangle = \beta \varepsilon_\infty^{2/3} (L_\infty Y_S)^{2/3}$ with $\beta \approx 1.8$ according to the theory (Hunt 1984*b*; Magnaudet 2003). Using the slope of the curve plotted in figure 9 and the value of ε_{Kav}^+ given above yields a slighly higher value $\beta \approx 2.0$ in the present flow. From the above results, the vertical integral scale is found to evolve as ${}^x L_v / L_\infty = \pi(\gamma/\beta) Y_S$ close to the surface. The present LES results suggest a value of $\alpha = \pi\gamma/\beta$ between 1.6 and 1.9 while the theory predicts $\alpha = 1.96$ (Hunt 1984*b*).

The HG theory also predicts that the difference between the surface value and the local value of the r.m.s. tangential velocities evolves as $\varepsilon_\infty^{1/3} (L_\infty Y_S)^{1/3}$ when $Y_S \to 0$ (see also Magnaudet 2003). Figure 10 shows the evolution of $(u_S^{+2} - u^{+2})^{3/2}$ and $(w_S^{+2} - w^{+2})^{3/2}$ for $y \leqslant 0.2 L_\infty$ (the subscript S refers to the corresponding surface value). Both curves confirm the theoretical prediction for $Y_S \leqslant 0.1$, approximately. Nevertheless the range of Y_S within which this $Y_S^{1/3}$ scaling holds is narrow compared to what we found previously for the vertical velocity. This is also in line with the theory, which predicts that the next term in the expansion of u^{+2} and w^{+2} vs. Y_S is linear, hence limiting the validity of the leading-order expansion, whereas no such term exists in the expansion of the vertical velocity (see the discussion in appendix A of Magnaudet 2003). This linear term is due to the distortion of the large-scale motions by the surface and its sign is opposite to that of the $Y_S^{2/3}$ contribution. Owing to the action of the mean shear in the open-channel flow, there is more energy in the large scales of the streamwise component than in those of the spanwise one. Hence the numerical prefactor of the linear term is larger in u^{+2} than in w^{+2}, which explains why the curve of figure 10 corresponding to u^+ has a smaller slope (≈ 2.10) than that corresponding to $w^+ (\approx 3.03)$.

An important consequence of the linear term just mentioned is that the tangential r.m.s. velocities and the turbulent kinetic energy pass through a minimum within the surface-influenced region. Using a von Karmàn spectrum to model the free-stream turbulence, HG found that K decreases from the value $K_\infty = 3/2\mathscr{U}^2$ corresponding to $Y_S \to \infty$ to a minimum value 0.865 K_∞ reached at $Y_{Smin} \approx 0.27$, and then re-increases up to the surface where $K(Y_S = 0) = K_\infty$ again, since $\langle u'^2 \rangle (Y_S = 0) = \langle w'^2 \rangle (Y_S = 0) =$

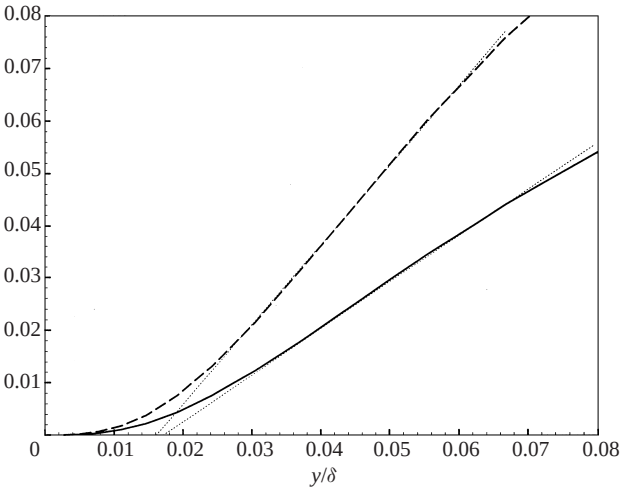

FIGURE 10. Evolution of tangential velocity fluctuations near the surface: ——, $(u_S^{+2} - u^{+2})^{3/2}$; — —, $(w_S^{+2} - w^{+2})^{3/2}$; - - - - -, $(v_{iS}^{+2} - v_i^{+2})^{3/2} \propto y/\delta$ ($i = 1$ or 3).

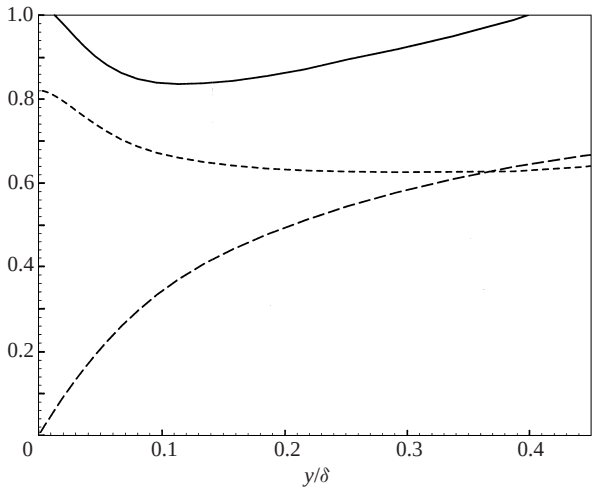

FIGURE 11. Evolution of the turbulent kinetic energy in the surface-influenced region: ——, K/K_∞; — —, v^+; – – –, w^+.

$(3/2)u^2$. The profile of K/K_∞ found in our LES is plotted in figure 11. The ratio of K/K_∞ is found to be less than unity over the whole range $0 < Y_S < 1$ (corresponding to $0.05 < y/\delta < 0.4$); it reaches a minimum $K_{min}/K_\infty \approx 0.84$ located at $Y_{Smin} \approx 0.22$, and recovers its 'free-stream' value within the viscous sublayer at $y/\delta \approx 0.02$. Clearly, this evolution agrees quantitatively well with the predictions of HG, bearing in mind that the theory assumes isotropic turbulence in the free stream and neglects any influence of the viscous sublayer.

6. Summary and conclusions

We have used the large-eddy simulation approach to produce statistical data concerning the turbulent field in the surface-influenced region of a statistically steady high-Reynolds-number open-channel flow. Comparisons with low-Reynolds-number DNS results were made possible via a re-scaling. In particular we showed that the

appropriate length scale of all near-surface quantities related to vorticity fluctuations is the Taylor microscale and not the viscous scale $\nu/u*$. This is simply a consequence of the fact that at high enough Reynolds number, the near-surface turbulence has lost the memory of the bottom boundary layer within which it was generated. At high Reynolds number, the turbulent kinetic energy budget near the surface was found to be dominated by dissipation and turbulent transport which brings energy towards the surface. Pressure-diffusion was found to play a significant role by lowering the net transport in the major part of the surface-influenced layer, and by increasing it very close to the surface. In line with available DNS results, the dissipation was found to exhibit a sharp minimum at the free surface. The fact that the correct dissipation profile close to the surface is recovered through a LES in which most of the small-scale processes are not resolved confirms that near-surface dissipation is essentially governed by viscous effects affecting the large-scale motions. Since the anisotropy of the turbulence entering the surface region decreases significantly as the Reynolds number increases, the pressure–strain correlations found in the present LES exhibit interesting differences compared to the low-Reynolds-number situation. In particular, energy from the normal r.m.s. velocity is redistributed almost equally between the two tangential components, whereas the spanwise component is favoured at low Reynolds number. Overall, comparison with available low-Reynolds-number data showed that the intercomponent energy transfer is very sensitive to the anisotropy of the turbulent field entering the surface-influenced layer.

We carried out a systematic comparison between the predictions of the HG theory and LES statistical results in the surface-influenced layer. Numerical results and theoretical predictions concerning one-dimensional spectra, integral length scales and r.m.s. velocities were found to be in very good agreement. In particular, the evolution of the low-wavenumber subrange of all three components of the numerical one-dimensional velocity spectra agrees very well with the theory. As a result, the normal r.m.s. velocity predicted by the LES is proportional to $Y_S^{1/3}$ over most of the source layer and the proportionality coefficient is close to its theoretical value. Variations of the turbulent kinetic energy within the source layer also agree with HG's predictions, especially concerning the position and amplitude of the minimum of the TKE.

Overall, the present numerical results indicate that outside the viscous sublayer, the HG theory, which was initially derived for studying the short-time evolution of shearless turbulence in the presence of an impermeable boundary, also provides an accurate description of the flow at long time. This conclusion contrasts with that of a low-Reynolds-number computational investigation (Perot & Moin 1995), where it was claimed that the description corresponding to the HG theory is only valid at short times following boundary insertion. Despite the evidence provided by the present numerical results, the fundamental reason for this agreement remains unknown at present. In particular, it is obvious from the results concerning the turbulent kinetic energy balance and the pressure–strain correlations discussed at § 4 that the long-time dynamics of the flow are dominated by nonlinear processes. Since such processes are not taken into account in the rapid distortion approximation, how can the HG theory remains valid at long time? To clarify this important question, several theoretical aspects of the problem are revisited in a companion paper (Magnaudet 2003). In brief, the crucial point appears to be that for large enough turbulent Reynolds number, the velocity correction induced by the presence of the surface is dominated at all time by the irrotational contribution evaluated by HG, i.e. rotational corrections remain weak outside the viscous sublayer. This argument explains why low-Reynolds-number

DNS data disagree with HG's predictions at long time while high-Reynolds-number experimental and LES results closely follow these predictions. Moreover it may be shown (Magnaudet 2003) that the leading surface-induced correction to the pressure field derives from a Bernoulli-like equation incorporating all the dominant linear and nonlinear processes associated with the presence of the surface. This is the basic reason why the HG predictions are compatible with the turbulent transport and intercomponent energy transfer mechanisms described in the present investigation.

The computer resources used in this work were provided by the Institut pour le Développement des Ressources en Informatique Scientifique (IDRIS/CNRS). We are indebted to the IDRIS staff and the Computer Service of the Institut de Mécanique des Fluides de Toulouse for their constant technical support.

REFERENCES

Batchelor, G. K. 1953 *The Theory of Homogeneous Turbulence*. Cambridge University Press.

Borue, V., Orszag, S. A. & Staroselsky, I. 1995 Interaction of surface waves with turbulence: direct numerical simulations of turbulent open-channel flow. *J. Fluid Mech.* **286**, 1–23.

Brumley, B. H. & Jirka, G. H. 1987 Near surface turbulence in grid-stirred tank. *J. Fluid Mech.* **183**, 235–263.

Brumley, B. H. & Jirka, G. H. 1988 Air-water transfer of slightly soluble gases: turbulence, interfacial processes and conceptual models. *PhysicoChem. Hydrodyn.* **10**, 295–319.

Calmet, I. & Magnaudet, J. 1997 Large-eddy simulation of high-Schmidt number mass transfer in a turbulent channel flow. *Phys. Fluids* **9**, 438–455 (referred to herein as CM).

Germano, M., Piomelli, U., Moin, P. & Cabot, W. 1991 A dynamic subgrid-scale eddy viscosity model. *Phys. Fluids* A **3**, 1760–1765.

Gibson, M. M. & Launder, B. E. 1978 Ground effects on pressure fluctuations in the atmospheric boundary layer. *J. Fluid Mech.* **86**, 491–511.

Handler, R. A., Saylor, J. R., Leighton, R. I. & Rovelstad, A. L. 1999 Transport of a passive scalar at a shear-free boundary in fully developed turbulent open channel flow. *Phys. Fluids* **11**, 2607–2625.

Handler, R. A., Swean, T. F., Leighton, R. I. & Swearingen, J. D. 1993 Length scales and the energy balance for turbulence near a free surface. *AIAA J.* **31**, 1998–2007.

Hannoun, I. A., Fernando, H. J. S. & List, E. J. 1988 Turbulence structure near a sharp interface. *J. Fluid Mech.* **189**, 189–209.

Hunt, J. C. R. 1984*a* Turbulence structure and turbulent diffusion near gas-liquid interfaces. In *Gas Transfer at Water Surfaces* (ed. W. Brutsaert & G. H. Jirka), pp. 67–82. Reidel.

Hunt, J. C. R. 1984*b* Turbulence structure in thermal convection and shear-free boundary layers. *J. Fluid Mech.* **138**, 161–184.

Hunt, J. C. R. & Graham, J. M. R. 1978 Free stream turbulence near plane boundaries. *J. Fluid Mech.* **84**, 209–235 (referred to herein as HG).

Komori, S., Murakami, Y. & Ueda, H. 1989 The relationship between surface-renewal and bursting motions in an open-channel flow. *J. Fluid Mech.* **203**, 103–123.

Komori, S., Nagaosa, R. & Murakami, Y. 1990 Mass transfer into a turbulent liquid across the zero-shear gas-liquid interface. *AIChE J.* **36**, 957–960.

Komori, S., Nagaosa, R., Murakami, Y., Chiba, S., Ishii, K. & Kuwahara, K. 1993 Direct numerical simulation of three-dimensional open-channel flow with zero-shear gas-liquid interface. *Phys. Fluids* A **5**, 115–125.

Komori, S., Ueda, H., Ogino, F. & Mizushina, T. 1982 Turbulence structure and transport mechanism at the free surface of an open channel flow. *Intl J. Heat Mass Transfer* **25**, 513–521.

Kumar, S., Gupta, R. & Banerjee, S. 1998 An experimental investigation of the characteristics of free-surface turbulence in channel flow. *Phys. Fluids* **10**, 437–456.

Lam, K. & Banerjee, S. 1992 On the condition of streak formation in a bounded turbulent flow. *Phys. Fluids* A **4**, 306–320.

Launder, B. E., Reece, G. J. & Rodi, W. 1975 Progress in the development of a Reynolds-stress turbulence closure. *J. Fluid Mech.* **68**, 537–565.

Leighton, R. I., Swean T. F., Handler R. A. & Swearingen, J. D. 1991 Interaction of vorticity with a free surface in turbulent open channel flow. *AIAA Paper* 91-0236.

Magnaudet, J. 2003 High-Reynolds-number turbulence in a shear-free boundary layer: revisiting the Hunt–Graham theory. *J. Fluid Mech.* (to appear).

McDougall, T. J. 1979 Measurements of turbulence in a zero-mean-shear mixed layer. *J. Fluid Mech.* **94**, 409–431.

Moin, P. & Kim, J. 1982 Numerical investigation of turbulent channel flow. *J. Fluid Mech.* **118**, 341–377.

Monin, A. S. & Yaglom, A. M. 1975 *Statistical Fluid Mechanics*, Vol. 2. MIT Press.

Nagaosa, R. 1999 Direct numerical simulation of vortex structures and turbulent scalar transfer across a free surface in a fully developed turbulence. *Phys. Fluids* **11**, 1581–1595.

Nagaosa, R. & Saito, T. 1997 Turbulence structure and scalar transfer in stratified free-surface flows. *AIChE J.* **43**, 2393–2404.

Nakagawa, H. & Nezu, I. 1977 Predictions of the contributions to the Reynolds stress from the bursting events in open-channel flows. *J. Fluid Mech.* **80**, 99–128.

Nakagawa, H. & Nezu, I. 1981 Structure of space-time correlations of bursting phenomena in open-channel flows. *J. Fluid Mech.* **104**, 1–43.

Nezu, I. & Rodi, W. 1986 Open channel flow measurements with a laser Doppler anemometer. *J. Hydraulic Engng* **112**, 335–355.

Pan, Y. & Banerjee, S. 1995 A numerical study of free surface turbulence in channel flow. *Phys. Fluids* **7**, 1649–1664.

Perot, B. & Moin, P. 1995 Shear-free turbulent boundary layers. Part 1. Physical insights into near-wall turbulence. *J. Fluid Mech.* **295**, 199–227.

Rashidi, M. 1997 Burst-turbulence interactions in free surface turbulent flows. *Phys. Fluids* **9**, 3485–3501.

Rashidi, M. & Banerjee, S. 1988 Turbulence structure in free-surface channel flows. *Phys. Fluids* **31**, 2491–2503.

Salvetti, M. V. & Banerjee, S. 1995 A *priori* tests of a new dynamic subgrid-scale model for finite-difference large-eddy simulations. *Phys. Fluids* **7**, 2831–2847.

Salvetti, M. V., Zang, Y., Street, R. L. & Banerjee, S. 1997 Large-eddy simulation of free-surface decaying turbulence with dynamic subgrid-scale models. *Phys. Fluids* **9**, 2405–2419.

Sarpkaya, T. 1996 Vorticity, free surface, and surfactants. *Annu. Rev. Fluid Mech.* **28**, 83–128.

Shen, L., Zhang, X., Yue, D. K. P. & Triantafyllou, G. S. 1999 The surface layer for free-surface turbulent flows. *J. Fluid Mech.* **386**, 167–212.

Swean, T. F., Leighton, R. I., Handler, R. A. & Swearingen, J. D. 1991 Turbulence modeling near the free surface in an open channel flow. *AIAA Paper* 91-0613 (referred to herein as SLHS).

Teixeira, M. A. C. & Belcher, S. E. 2000 Dissipation of shear-free turbulence near boundaries. *J. Fluid Mech.* **422**, 167–191.

Tennekes, N. H. & Lumley, J. L. 1972 *A First Course in Turbulence*. MIT Press.

Thomas, N. H. & Hancock, P. E. 1977 Grid turbulence near a moving wall. *J. Fluid Mech.* **82**, 481–496.

Walker, D. T., Leighton, R. I. & Garza-Rios, L. O. 1996 Shear-free turbulence near a flat free surface. *J. Fluid Mech.* **320**, 19–51.

Wu, J. Z. 1995 A theory of three-dimensional interfacial vorticity dynamics. *Phys. Fluids* **7**, 2375–2395.

Zang, Y., Street, R. L. & Koseff, J. R. 1993 A dynamic mixed subgrid-scale model and its application to turbulent recirculating flows. *Phys. Fluids* A **5**, 3186–3196.